Progress In Electromagnetics Research B, Vol. 55, 151–168, 2013

TWO-DIMENSIONAL PATTERN SYNTHESIS OF STACKED CONCENTRIC CIRCULAR ANTENNA ARRAYS USING BEE COLONY ALGORITHMS

Song-Han Yang and Jean-Fu Kiang*

Department of Electrical Engineering, Graduate Institute of Communication Engineering, National Taiwan University, Taipei, Taiwan

Abstract—Stacked concentric circular antenna arrays (SCCAA's) supporting both the scanning mode and the tracking mode are optimized in both the azimuth and elevation planes. The gbest-guided artificial bee colony algorithm (GABCA) is adopted to optimize the dual-mode field patterns of thinned SCCAA's. Performance comparison of the GABCA with conventional ABCA and particle swarm optimization (PSO) algorithms is also presented.

1. INTRODUCTION

Circular antenna arrays (CAA's) have received much attention in mobile communications, satellite links, navigation aids, and so on [1]. The main concerns with these arrays include side-lobe suppression, location of nulls, beam-width control, and directivity enhancement [2–6].

The synthesis of antenna patterns often involves a non-convex optimization. Different evolutionary algorithms (EA's) have been proposed to search for the global optimal solution in such complicated electromagnetic problems. Panduro et al. apply a genetic algorithm (GA) to optimize the amplitude and location of all the elements in a CAA, to reduce the side-lobe level while maintaining the beamwidth [2]. Shihab et al. report that a CAA can be optimized using a particle swarm optimization (PSO) algorithm, to achieve a lower side-lobe level using a smaller array [3]. Panduro et al. compare the optimization methods of GA, PSO and differential evolution strategy (DES) ones, in suppressing the side-lobe level and increasing the directivity of a CAA [4]. Roy et al. adopt a modified invasive weed optimization (IWO) algorithm to reduce the side-lobe level,

Received 24 July 2013, Accepted 26 September 2013, Scheduled 27 September 2013
* Corresponding author: Jean-Fu Kiang (jfkiang@cc.ee.ntu.edu.tw).

increase the directivity, and control the null locations of a CAA [5]. Basu and Mahanti apply a firefly algorithm to reduce the side-lobe level of a thinned two-ring concentric circular antenna array (CCAA), constrained with a given beamwidth [6]. Cylindrical arrays have also been designed to achieve narrow beamwidth and low side-lobe level in the azimuth plane [7]. In these tasks, the field patterns in both the azimuth and the elevation planes are not optimized simultaneously.

In this work, a stacked concentric circular antenna array (SCCAA), which is a hybrid of CCAA and cylindrical array, is synthesized and studied. The goal is optimizing the radiation pattern in the azimuth plane while reducing the beamwidth in the elevation plane. This SCCAA is designed to operate in both the scanning mode and the tracking mode in the azimuth plane. A gbest-guided artificial bee colony algorithm (GABCA) [8] is adopted to optimize the amplitude and phase of the elements in the SCCAA. Conventional ABCA and PSO methods are also used to compare the optimization results and the performance of the GABCA.

This paper is organized as follows. The GABCA and the ABCA algorithms are briefly reviewed in Section 2, the techniques of generating the sum and the difference patterns for SCCAA's are described in Section 3, pattern synthesis in both the azimuth and the elevation planes, using GABCA, ABCA and PSO, is discussed in Section 4, followed by the conclusion in Section 5.

2. BRIEF REVIEW OF THE ARTIFICIAL BEE COLONY ALGORITHM

The artificial bee colony algorithm (ABCA) is a derivative-free optimization algorithm, which is inspired by the foraging behavior of a honey-bee swarm [8]. The ABCA has been successfully applied to many problems, including array synthesis and steel production [9, 10]. When applied to an optimization problem, each bee searches for a new food source (solution vector) with the most nectar amount, also known as the global optimum. In order to improve the search capability, Zhu and Kwong [8] propose a gbest-guided artificial bee colony algorithm (GABCA), by exploiting the information in the global solution of a particle swarm optimization (PSO) technique [11]. Consecutive phases of the GABCA used in this work is briefly reviewed below.

2.1. Initialization

The number of employed bees and onlookers, as well as the number of food sources, are set equal to SN. After $\text{trail}_{\max}$ times of trial failures

on a specific food source, the search will be abandoned. The food source matrix has the explicit form of

$$\bar{\bar{X}} = \begin{bmatrix} \bar{x}_1 \\ \bar{x}_2 \\ \vdots \\ \bar{x}_S \end{bmatrix} = \begin{bmatrix} x_{11} & x_{12} & \dots & x_{1D} \\ x_{21} & x_{22} & \dots & x_{2D} \\ \vdots & \vdots & \dots & \vdots \\ x_{S1} & x_{S2} & \dots & x_{SD} \end{bmatrix}$$

where S is the number of food sources, D the dimension of the solution vector, and each row in the matrix records the position of one particular food source.

The GABCA generates a randomly distributed positions of S food sources as

$$\bar{\bar{X}}^{(1)} = X_{\min} + (X_{\max} - X_{\min})\text{rand}(S, D)$$

where rand(S, D) returns an $S \times D$ matrix of random numbers, all picked from the interval [0, 1]; $X_{\min}$ and $X_{\max}$ are the lower and the upper bounds, respectively, of the positions.

2.2. The Employed Bees Phase

A proper fitness value is defined as a function of the bee position, based on which the bees can trace the optimal solution. Each employed bee searches for a new food source in the neighborhood of its present position, $\bar{x}_m$. The updated coordinate, $\bar{x}_{\text{new}}[d]$, with $d = 1, 2, \dots, D$, is derived as

$$\bar{x}_{\text{new}}[d] = \bar{x}_m[d] + (2 \times \text{rand} - 1)\,(\bar{x}_k[d] - \bar{x}_m[d]) \tag{1}$$

where k is randomly picked from $\{1, 2, \dots, S\}$, and is different from m.

Equation (1) can be expedited by making use of the global best solution vector, $\bar{g}$, as [8]

$$\begin{aligned} \bar{x}_{\text{new}}[d] \;=\; & \bar{x}_m[d] + (2 \times \text{rand} - 1)\,(\bar{x}_k[d] - \bar{x}_m[d]) \\ & +1.5 \times \text{rand}\,(\bar{g}[d] - \bar{x}_m[d]) \end{aligned} \tag{2}$$

which will help the bees to move towards a better position with higher fitness value. If the fitness value (nectar amount) of $\bar{x}_{\text{new}}$ is better than that of $\bar{x}_m$, $\bar{x}_{\text{new}}$ will replace $\bar{x}_m$. Otherwise, $\bar{x}_{\text{new}}$ will be discarded.

2.3. The Onlookers Phase

An onlooker bee sets target on a food source, $\bar{x}_m$, with probability p_m, and updates its $\bar{x}_{\text{new}}$ using the same method as the employed bees. The probability, p_m, is determined as

$$p_m = \frac{F_m}{\sum_{m=1}^{\text{SN}} F_m} \tag{3}$$

where F_m is the fitness value at $\bar{x}_m$. A better (larger) F_m implies a higher probability that $\bar{x}_m$ is updated.

In the employed bees phase, each food source attracts one employed bee. In the onlookers phase, a better food source may attract more than one onlooker bees, and a worse food source may attract none at all.

2.4. The Scouts Phase

A food source around $\bar{x}_m$ will be abandoned if a bee cannot update the position with better fitness after $\text{trial}_{\max}$ times of fitness iterations. Under such circumstances, the scout bee is assigned a new food source at

$$\bar{x}_{\text{scout}} = X_{\min} + (X_{\max} - X_{\min}) \, \text{rand}(1, D)$$

to replace $\bar{x}_m$, where $\text{rand}(1, D)$ returns an $1 \times D$ array of random numbers, all picked from the interval $[0, 1]$. This is an analog to the mutation step in a typical GA.

3. ARRAY PATTERNS OF STACKED CONCENTRIC CIRCULAR ANTENNA ARRAYS

Figure 1 shows the geometrical configuration of an SCCAA, which is consisted of P layers of CCAA's. Each layer of CCAA is composed of M concentric rings, the mth ring has a radius of r_m and contains N_m elements equally spaced along the circumference.

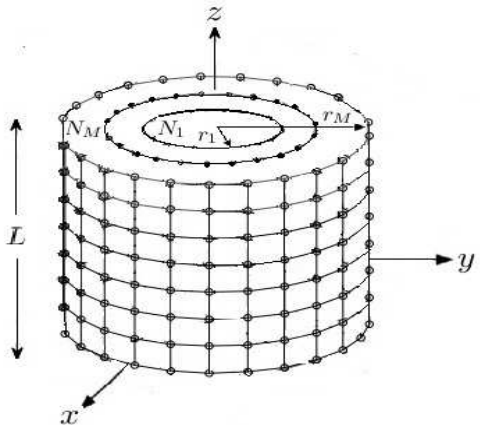

Figure 1. Geometry of a stacked concentric circular antenna array.

The array factor of a single layer of CCAA, with the main beam pointing in the (θ_0, ϕ_0) direction, can be expressed as [7]

$$\mathrm{AF}_c(\theta,\phi) = \sum_{m=1}^{M}\sum_{n=1}^{N_m} a_{mn} e^{jkr_m[\sin\theta\cos(\phi-\phi_{mn})-\sin\theta_0\cos(\phi_0-\phi_{mn})]+j\alpha_{mn}} \quad (4)$$

where a_{mn} and α_{mn} are the amplitude and phase, respectively, of the nth element on the mth ring, k is the wavenumber, and ϕ_{mn} is angular position of the nth element on the mth ring. The radius, r_m, and the phase, ϕ_{mn}, can be expressed as

$$kr_m = \frac{2\pi r_m}{\lambda} = \sum_{\alpha=1}^{N_m} d_\alpha^m$$

$$\phi_{mn} = \frac{2\pi}{\sum_{\alpha=1}^{N_m} d_\alpha^m} \sum_{\alpha=1}^{n} d_\alpha^m = \frac{2\pi}{kr_m} \sum_{\alpha=1}^{n} d_\alpha^m$$

where d_n^m is the arc spacing between elements n and $n-1$ on the mth ring.

If the amplitude of the feeding signal to the mnth element in the pth CCAA layer is that of the mnth element in the first CCAA layer multiplied by a constant, c_p, the array pattern of the SCCAA can be decomposed into

$$\mathrm{AF}(\theta,\phi) = \mathrm{AF}_z(\theta,\phi)\mathrm{AF}_c(\theta,\phi) \quad (5)$$

where AF_z is the array pattern with P elements along the z direction, at a uniform spacing ℓ. Explicitly,

$$\mathrm{AF}_z(\theta,\phi) = \sum_{p=1}^{P} c_p e^{jk(p-1)\ell\cos\theta}$$

3.1. Stacked Concentric Circular Taylor Array

The Taylor circular aperture distribution is designed to generate a sum pattern [12], which is adopted as the initial guess before optimization. If the main beam is pointing in $(\theta_0, \phi_0) = (0^\circ, 0^\circ)$, the far-field pattern has $N_b - 1$ nulls over $0 < \theta \le 90^\circ$ in the x-z plane, and all the side-lobe intensities are below a specified level.

The required circular aperture distribution can be represented as [12]

$$E_{N_b}(r) = \sum_{m=0}^{N_b-1} B_m J_0(\pi\delta_m r), \qquad \left|\frac{r}{a}\right| \le 1 \quad (6)$$

where δ_m's satisfy the condition $J_1(\pi\delta_m) = 0$ [12], $B_0 = 1$, $J_0(\alpha)$ and $J_1(\alpha)$ are Bessel functions of the zeroth and the first order, respectively,

$$B_m = \frac{-\prod_{n_b=1}^{N_b-1}\left[1-\delta_m^2/Z_{n_b}^2\right]}{J_0(\pi\delta_m)\prod_{n_b=0,n_b\neq m}^{N_b-1}\left[1-\delta_m^2/\delta_{n_b}^2\right]}, \qquad 1 \le m \le N_b - 1$$

and

$$Z_{n_b} = \delta_{N_b}\sqrt{\frac{A^2+(n_b-0.5)^2}{A^2+(N_b-0.5)^2}}$$

with

$$A = \frac{\cosh^{-1}\left(10^{\mathrm{SLL}/20}\right)}{\pi}$$

in which the side-lobe level (SLL) is in unit of dB.

Before optimization, the amplitudes, a_{mn}'s, in (4) are sampled from the Taylor circular aperture distribution [14], and the phases, α_{mn}'s, in (4) are set to zero. An example of the Taylor circular aperture distribution, with $N_b = 6$ and SLL = 20 dB, is shown in Fig. 2.

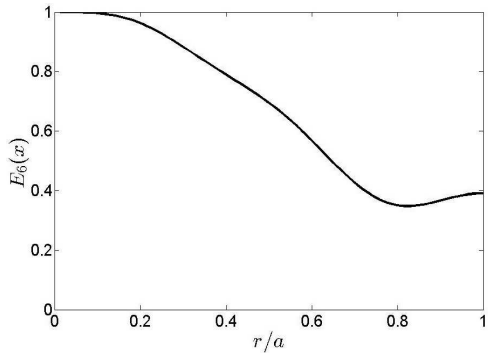

Figure 2. Taylor aperture distribution with $\phi = 0$, $N_b = 6$ and SLL = 20 dB.

3.2. Stacked Concentric Circular Bayliss Array

The Bayliss circular aperture distribution is designed to generate a null in the boresight direction [12]. If $(\theta_0, \phi_0) = (0°, 0°)$, the far-field pattern will have a null in the z direction, and also $N_b - 1$ nulls over

$0 < \theta \leq 90^\circ$ in the x-z plane; and all the side-lobes are below a specified level.

The required circular aperture distribution can be represented as [12]

$$E_{N_b}(r,\phi) = \cos\phi \sum_{m=0}^{N_b-1} B_m J_1(\pi\sigma_m r), \qquad \left|\frac{r}{a}\right| \leq 1 \tag{7}$$

where σ_m's are the zeros of the Bessel function, with $J_1'(\pi\sigma_m) = 0$ [12],

$$B_m = \frac{\sigma_m^2}{J_1(\pi\sigma_m)} \frac{\prod_{n_b=1}^{N_b-1}\left(1-\sigma_m^2/Z_{n_b}^2\right)}{\prod_{n_b=0,n_b\neq m}^{N_b-1}\left(1-\sigma_m^2/\sigma_{n_b}^2\right)}$$

$$Z_{n_b} = \begin{cases} \sigma_{N_b}\sqrt{\dfrac{\xi_{n_b}^2}{A^2+N_b^2}}, & 1 \leq n_b \leq 4 \\ \sigma_{N_b}\sqrt{\dfrac{A^2+n_b^2}{A^2+N_b^2}}, & 5 \leq n_b \leq N_b-1 \end{cases}$$

The coefficients, ξ_n and A, are calculated as

$$\xi_{n_b} = \sum_{p=0}^{4} C_p^{n_b} (\mathrm{SLL})^p$$

$$A = \sum_{p=0}^{4} C_p^{A} (\mathrm{SLL})^p$$

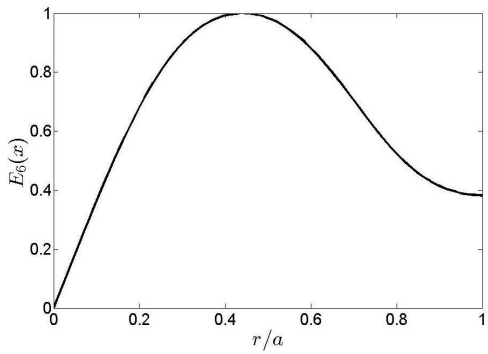

Figure 3. Bayliss aperture distribution with $\phi = 0$, $N_b = 6$ and SLL = 20 dB.

where SLL is in unit of dB, and the coefficients C_p's are listed in [13].

Before optimization, the amplitudes, a_{mn}'s, in (4) are sampled from the Bayliss circular aperture distribution [14], and the phases, α_{mn}'s, in (4) are set to zero. An example of the Bayliss circular aperture distribution, with $N_b = 6$ and SLL $= 20$ dB, is shown in Fig. 3.

3.3. Characteristics of Dual-mode Stacked Concentric Circular Arrays

Consider a dual-mode CCAA, with $M = 6$, $r_M = 48.27\lambda$, a ring spacing of 0.9λ, and an approximate arc spacing of 1.25λ within each ring. This CCAA is designated as $A_r(0.9,\ 1.25,\ 0)$, where r stands for regular. The first, the second, and the third arguments in the parenthesis record the ring spacing, the approximate arc spacing within each ring, and the uniform spacing between adjacent layers, respectively. The SCCAA's with uniform layer spacing of 0.5λ, 1λ and

Table 1. Simulated characteristics of SCCAA's before optimization.

azimuth plane

Type	M	N_m	P	N_T	L (λ)
$A_r(0.5,\ 0.5,\ 0)$	10	40 46 52 58 65 71 77 83 90 96	1	678	0
$A_r(0.9,\ 1.25,\ 0)$	6	16 20 25 29 34 38	1	162	0
$A_r(0.9,\ 1.25,\ 0.5)$	6	16 20 25 29 34 38	3	486	1
$A_r(0.9,\ 1.25,\ 1.0)$	6	16 20 25 29 34 38	3	486	2
$\mathbf{A_r(0.9,\ 1.25,\ 1.5)}$	**6**	**16 20 25 29 34 38**	**3**	**486**	**3**
Type	BW_s^a (°)	SA_d^a (°)	P_s^a (dB)	P_d^a (dB)	$D_{\max}$ (dB)
$A_r(0.5,\ 0.5,\ 0)$	8.40	6.00	−13.37	−14.26	19.40–20.76
$A_r(0.9,\ 1.25,\ 0)$	8.40	5.80	−14.31	−9.88	19.40–24.88
$A_r(0.9,\ 1.25,\ 0.5)$	8.40	5.80	−14.31	−9.88	19.40–25.56
$A_r(0.9,\ 1.25,\ 1.0)$	8.40	5.80	−14.31	−9.88	19.95–27.23
$\mathbf{A_r(0.9,\ 1.25,\ 1.5)}$	**8.4**	**5.80**	**−14.31**	**−9.88**	**21.76–28.82**

elevation plane

Type	M	N_m	P	N_T	L (λ)
A_r(0.5, 0.5, 0)	10	40 46 52 58 65 71 77 83 90 96	1	678	0
A_r(0.9, 1.25, 0)	6	16 20 25 29 34 38	1	162	0
A_r(0.9, 1.25, 0.5)	6	16 20 25 29 34 38	3	486	1
A_r(0.9, 1.25, 1.0)	6	16 20 25 29 34 38	3	486	2
$\mathbf{A_r}$(0.9, 1.25, 1.5)	**6**	**16 20 25 29 34 38**	**3**	**486**	**3**
Type	BW_s^e (°)	—	P_s^e (dB)	—	$D_{\max}$ (dB)
A_r(0.5, 0.5, 0)	44.20	–	−13.37	—	19.40–20.76
A_r(0.9, 1.25, 0)	44.20	—	−14.31	—	19.40–24.88
A_r(0.9, 1.25, 0.5)	44.20	—	−21.26	—	19.40–25.56
A_r(0.9, 1.25, 1.0)	39.00	—	−14.77	—	19.95–27.23
$\mathbf{A_r}$(0.9, 1.25, 1.5)	**25.60**	—	**−16.90**	—	**21.76–28.82**

$r_M = 48.27\lambda$, $P = 3$ and $(\theta_0, \phi_0) = (90°, 0°)$.

1.5λ, respectively, are also considered; labeled as A_r(0.9, 1.25, 0.5), A_r(0.9, 1.25, 1) and A_r(0.9, 1.25, 1.5), respectively.

The characteristics of A_r(0.9, 1.25, 0), A_r(0.9, 1.25, 0.5), A_r(0.9, 1.25, 1) and A_r(0.9, 1.25, 1.5) with $P = 3$ and $P = 5$ are summarized in Tables 1 and 2, respectively; where BW_s^a (°) is the beamwidth of the sum pattern, and SA_d^a (°) is the squint angle of the difference pattern, both in the azimuth plane; P_s^a (dB) and P_d^a (dB) are the maximum side-lobe level of the sum pattern and the difference pattern, respectively, in the azimuth plane. Similarly, BW_s^e (°) and P_s^e (dB) are the beamwidth and the maximum side-lobe level, respectively, of the sum pattern in the elevation plane.

With the array pattern characterized in (5), the SCCAA will have roughly the same beamwidth and side-lobe level in the azimuth plane, as those of the CCAA. In the elevation plane, however, the beamwidth and side-lobe level of the SCCAA becomes smaller than their counterpart of the CCAA. With more layers stacked, the maximum directivity of the SCCAA is also increased [15].

4. OPTIMIZATION OF STACKED CONCENTRIC CIRCULAR ANTENNA ARRAYS

The design goal is to enable the same SCCAA to radiate either the sum pattern or the difference pattern, pending on the excitation signals. The side-lobe level is minimized, while the beamwidth of the sum pattern and the squint angle of the difference pattern are preserved. To achieve these requirements, the fitness function is designed as

$$f\left(\bar{w}_s, \bar{w}_d, \bar{\psi}_s, \bar{\psi}_d\right) = f^a\left(\bar{w}_s, \bar{w}_d, \bar{\psi}_s, \bar{\psi}_d\right) + f^e\left(\bar{w}_s, \bar{w}_d, \bar{\psi}_s, \bar{\psi}_d\right) \quad (8)$$

where the first term and the second term on the right hand side of (8) are used to specify the patterns in the azimuth plane and the elevation plane, respectively; $\bar{w}_s = [w_{s1}, w_{s2}, \ldots, w_{sN}]^t$, $\bar{\psi}_s = [\psi_{s1}, \psi_{s2}, \ldots, \psi_{sN}]^t$, $\bar{w}_d = [w_{d1}, w_{d2}, \ldots, w_{dN}]_d^t$ and $\bar{\psi}_d = [\psi_{d1}, \psi_{d2}, \ldots, \psi_{dN}]^t$; w_{sn} and ψ_{sn} are the amplitude and the phase, respectively, on the nth antenna element when the sum pattern is generated; w_{dn} and ψ_{dn} are the amplitude and the phase, respectively, on the nth antenna element when the difference pattern is generated. The amplitude and the phase on all the elements are allowed to vary

Table 2. Simulated characteristics of SCCAA's before optimization.

azimuth plane

Type	M	N_m	P	N_T	L (λ)
A_r(0.5, 0.5, 0)	10	40 46 52 58 65 71 77 83 90 96	1	678	0
A_r(0.9, 1.25, 0)	6	16 20 25 29 34 38	1	162	0
A_r(0.9, 1.25, 0.5)	6	16 20 25 29 34 38	5	810	2
A_r(0.9, 1.25, 1.0)	6	16 20 25 29 34 38	5	810	4
$\mathbf{A_r}$(0.9, 1.25, 1.5)	**6**	**16 20 25 29 34 38**	**5**	**810**	**6**
Type	BW_s^a (°)	SA_d^a (°)	P_s^a (dB)	P_d^a (dB)	$D_{\max}$ (dB)
A_r(0.5, 0.5, 0)	8.40	6.00	−13.37	−14.26	19.40–20.76
A_r(0.9, 1.25, 0)	8.40	5.80	−14.31	−9.88	19.40–24.88
A_r(0.9, 1.25, 0.5)	8.40	5.80	−14.31	−9.88	19.40–26.75
A_r(0.9, 1.25, 1.0)	8.40	5.80	−14.31	−9.88	22.40–29.37
$\mathbf{A_r}$(0.9, 1.25, 1.5)	**8.40**	**5.80**	**−14.31**	**−9.88**	**23.98–31.21**

elevation plane

Type	M	N_m	P	N_T	L (λ)
A_r(0.5, 0.5, 0)	10	40 46 52 58 65 71 77 83 90 96	1	678	0
A_r(0.9, 1.25, 0)	6	16 20 25 29 34 38	1	162	0
A_r(0.9, 1.25, 0.5)	6	16 20 25 29 34 38	5	810	2
A_r(0.9, 1.25, 1.0)	6	16 20 25 29 34 38	5	810	4
$\mathbf{A_r}$(0.9, 1.25, 1.5)	**6**	**16 20 25 29 34 38**	**5**	**810**	**6**
Type	BW_s^e (°)	—	P_s^e (dB)	—	$D_{\max}$ (dB)
A_r(0.5, 0.5, 0)	44.20	—	−13.37	—	19.40–20.76
A_r(0.9, 1.25, 0)	44.20	—	−14.31	—	19.40–24.88
A_r(0.9, 1.25, 0.5)	44.20	—	−28.74	—	19.40–26.75
A_r(0.9, 1.25, 1.0)	23.00	—	−14.77	—	22.40–29.37
$\mathbf{A_r}$(0.9, 1.25, 1.5)	**15.40**	—	**−13.01**	—	**23.98–31.21**

$r_M = 48.27\lambda$, $P = 5$ and $(\theta_0, \phi_0) = (90°, 0°)$.

in the range of $(0, 1]$ and $(-\pi, \pi]$, respectively.

The first term in (8) is further decomposed as

$$\begin{aligned} & f^a\left(\bar{w}_s, \bar{w}_d, \bar{\psi}_s, \bar{\psi}_d\right) \\ = \; & P_s^a\left(\Omega_s^a \left| \bar{w}_s, \bar{\psi}_s\right.\right) + P_d^a\left(\Omega_d^a \left| \bar{w}_d, \bar{\psi}_d\right.\right) \\ & + K\left|\mathrm{BW}_s^a\left(\bar{w}_s, \bar{\psi}_s\right) - \mathrm{BW}_{so}^a\right| + K\left|\mathrm{SA}_d^a\left(\bar{w}_d, \bar{\psi}_d\right) - \mathrm{SA}_{do}^a\right| \end{aligned} \quad (9)$$

where K is an empirical weighting factor. The first term and the second term on the right hand side of (9) are used to minimize the side-lobe level of the sum pattern and the difference pattern, respectively; where Ω_s^a and Ω_d^a indicate the angular locations of the maximum side-lobe level of the sum pattern and the difference pattern, respectively, in the azimuth plane. The third term on the right hand side of (9) is used to achieve the desired beamwidth, BW_{so}^a (°), of the sum pattern in the azimuth plane, measured from null to null. The last term on the right hand side of (9) is used to achieve the desired squint angle, SA_{do}^a (°), of the difference pattern in the azimuth plane.

Similarly, the second term in (8) is further decomposed as

$$f^e\left(\bar{w}_s, \bar{w}_d, \bar{\psi}_s, \bar{\psi}_d\right) = P_s^e(\Omega_s^e \left| \bar{w}_s, \bar{\psi}_s\right.) + K\left|\mathrm{BW}_s^e(\bar{w}_s, \bar{\psi}_s) - \mathrm{BW}_{so}^e\right| \quad (10)$$

where the first term and the second term on the right hand side are used to minimize the side-lobe level and to achieve the desired beamwidth, BW_{so}^{e} (°), respectively, of the sum pattern in the elevation plane; Ω_s^e indicates the angular location of the maximum side-lobe level of the sum pattern in the elevation plane.

For comparison, the particle swarm optimization (PSO) algorithm is also applied [11]. In the PSO algorithm, a whole swarm of 20 particles fly through the search space, based on the instructions of habit, self-knowledge and social-knowledge. Both the empirical constants in the updating equation, C_1 and C_2, are set to 2 [11]. The habit weight, w, decreases linearly, from 0.9 to 0.4, as the iteration proceeds. The invisible boundary condition (IBC) is adopted, and the

Table 3. Parameters used in GABCA and ABCA [8].

P	SN	D	$\mathrm{trial}_{\max}$	K	$\mathrm{BW}_{so}^{a}(^\circ)$	SA_{do}^{a} (°)	BW_{so}^{e} (°)
3	20	324	200	10^6	8.00	6.00	25.60
5	20	324	200	10^6	8.00	6.00	15.40

Table 4. Simulated characteristics of SCCAA's after optimization.

azimuth plane

Type	M	N_m	P	N_T	L (λ)
$A_r(0.5, 0.5, 0)$	10	40 46 52 58 65 71 77 83 90 96	1	678	0
$A_r(0.9, 1.25, 1.5)$	6	16 20 25 29 34 38	3	486	3
$\mathbf{A_g(0.9, 1.25, 1.5)}$	**6**	**16 20 25 29 34 38**	**3**	**486**	**3**
$A_a(0.9, 1.25, 1.5)$	6	16 20 25 29 34 38	3	486	3
$A_p(0.9, 1.25, 1.5)$	6	16 20 25 29 34 38	3	486	3
Type	BW_{s}^{a} (°)	SA_{d}^{a} (°)	P_s^a (dB)	P_d^a (dB)	$D_{\max}$ (dB)
$A_r(0.5, 0.5, 0)$	8.40	6.00	−13.37	−14.26	19.40–20.76
$A_r(0.9, 1.25, 1.5)$	8.40	5.80	−14.31	−9.88	21.76–28.82
$\mathbf{A_g(0.9, 1.25, 1.5)}$	**8.40**	**6.00**	**−17.07**	**−15.09**	**21.76–28.82**
$A_a(0.9, 1.25, 1.5)$	8.40	6.00	−14.35	−10.65	21.76–28.82
$A_p(0.9, 1.25, 1.5)$	8.40	6.00	−15.85	−13.48	21.76–28.82

elevation plane

Type	M	N_m	P	N_T	L (λ)
$A_r(0.5, 0.5, 0)$	10	40 46 52 58 65 71 77 83 90 96	1	678	0
$A_r(0.9, 1.25, 1.5)$	6	16 20 25 29 34 38	3	486	3
$\mathbf{A_g(0.9, 1.25, 1.5)}$	**6**	**16 20 25 29 34 38**	**3**	**486**	**3**
$A_a(0.9, 1.25, 1.5)$	6	16 20 25 29 34 38	3	486	3
$A_p(0.9, 1.25, 1.5)$	6	16 20 25 29 34 38	3	486	3
Type	BW$_s^e$ (°)	—	P_s^e (dB)	—	$D_{\max}$ (dB)
$A_r(0.5, 0.5, 0)$	44.20	—	−13.37	—	19.40–20.76
$A_r(0.9, 1.25, 1.5)$	25.60	—	−16.90	—	21.76–28.82
$\mathbf{A_g(0.9, 1.25, 1.5)}$	**25.60**	—	**−24.41**	—	**21.76–28.82**
$A_a(0.9, 1.25, 1.5)$	25.60	—	−17.13	—	21.76–28.82
$A_p(0.9, 1.25, 1.5)$	25.60	—	−19.51	—	21.76–28.82

$r_M = 48.27\lambda$, $P = 3$ and $(\theta_0, \phi_0) = (90°, 0°)$.

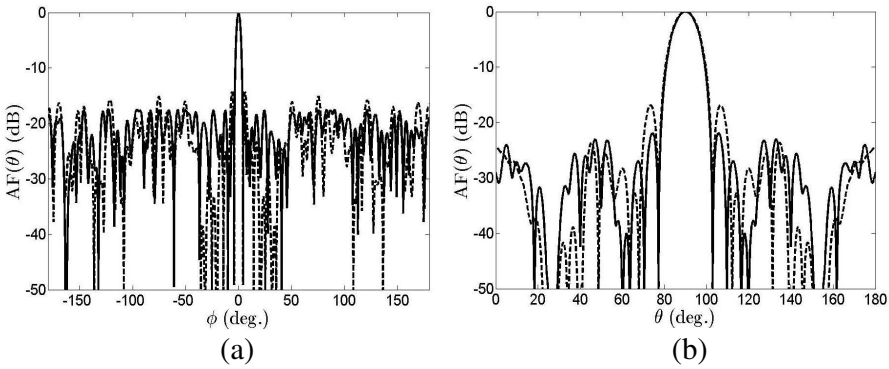

Figure 4. Sum pattern of dual-mode SCCAA's, (a) in the azimuth plane, (b) in the elevation plane, $(\theta_0, \phi_0) = (90°, 0°)$, $M = 6$, $r_M = 48.27\lambda$, $P = 3$, solid curve (—): $A_g(0.9, 1.25, 1.5)$, dashed curve (− − −): $A_r(0.9, 1.25, 1.5)$.

maximum velocity is set to 20% of the maximum coordinate in the search space.

By optimizing the amplitude and phase of elements in $A_r(0.9, 1.25, 1.5)$, another array, labeled as $A_\alpha(0.9,\ 1.25,\ 1.5)$, is obtained. The subscript, α, can be g, a or p, corresponding to the algorithms of GABCA, ABCA or PSO. The parameters used in the GABCA and the ABCA are listed in Table 3.

Other parameters related to $A_r(0.9,\ 1.25,\ 1.5)$ are $(\theta_0, \phi_0) = (90°, 0°)$, $M = 6$, $r_M = 48.27\lambda$ and $P = 3$. The optimized arrays, $A_g(0.9,\ 1.25,\ 1.5)$, $A_a(0.9,\ 1.25,\ 1.5)$ and $A_p(0.9,\ 1.25,\ 1.5)$ are derived, with their characteristics summarized in Tables 4 and 6. Figs. 4 and 5 show the field patterns in the azimuth and the elevation planes, respectively, of $A_r(0.9,\ 1.25,\ 1.5)$ and $A_g(0.9,\ 1.25,\ 1.5)$.

The arrays $A_r(0.5,\ 0.5,\ 0)$, $A_r(0.9,\ 1.25,\ 1.5)$ and $A_g(0.9,\ 1.25,\ 1.5)$ have similar BW_s^a and SA_s^a. The $A_r(0.5,\ 0.5,\ 0)$ has a better value of $P_s^a + P_d^a + P_s^e$ (in dB) than $A_r(0.9,\ 1.25,\ 1.5)$; while $A_r(0.9,\ 1.25,\ 1.5)$ outperforms $A_r(0.5,\ 0.5,\ 0)$ in BW_s^e and P_s^e. The optimized array, $A_g(0.9,\ 1.25,\ 1.5)$, with the initial condition of $A_r(0.9,\ 1.25,$

Table 5. Simulated characteristics of SCCAA's after optimization.

azimuth plane

Type	M	N_m	P	N_T	L (λ)
$A_r(0.5, 0.5, 0)$	10	40 46 52 58 65 71 77 83 90 96	1	678	0
$A_r(0.9, 1.25, 1.5)$	6	16 20 25 29 34 38	5	810	6
$\mathbf{A_g(0.9,\ 1.25,\ 1.5)}$	**6**	**16 20 25 29 34 38**	**5**	**810**	**6**
$A_a(0.9,\ 1.25,\ 1.5)$	6	16 20 25 29 34 38	5	810	6
$A_p(0.9,\ 1.25,\ 1.5)$	6	16 20 25 29 34 38	5	810	6
Type	BW_s^a (°)	SA_d^a (°)	P_s^a (dB)	P_d^a (dB)	$D_{\max}$ (dB)
$A_r(0.5, 0.5, 0)$	8.40	6.00	−13.37	−14.26	19.40–20.76
$A_r(0.9, 1.25, 1.5)$	8.40	5.80	−14.31	−9.88	23.98–31.21
$\mathbf{A_g(0.9,\ 1.25,\ 1.5)}$	**8.40**	**6.00**	**−17.57**	**−17.20**	**23.98–31.21**
$A_a(0.9,\ 1.25,\ 1.5)$	8.40	6.00	−13.79	−10.67	23.98–31.21
$A_p(0.9,\ 1.25,\ 1.5)$	8.40	6.00	−17.09	−14.64	23.98–31.21

elevation plane

Type	M	N_m	P	N_T	L (λ)
$A_r(0.5, 0.5, 0)$	10	40 46 52 58 65 71 77 83 90 96	1	678	0
$A_r(0.9, 1.25, 1.5)$	6	16 20 25 29 34 38	5	810	6
$\mathbf{A_g(0.9, 1.25, 1.5)}$	**6**	**16 20 25 29 34 38**	**5**	**810**	**6**
$A_a(0.9, 1.25, 1.5)$	6	16 20 25 29 34 38	5	810	6
$A_p(0.9, 1.25, 1.5)$	6	16 20 25 29 34 38	5	810	6
Type	BW_s^e (°)	—	P_s^e (dB)	—	$D_{\max}$ (dB)
$A_r(0.5, 0.5, 0)$	44.20	—	−13.37	—	19.40–20.76
$A_r(0.9, 1.25, 1.5)$	15.40	—	−13.01	—	23.98–31.21
$\mathbf{A_g(0.9, 1.25, 1.5)}$	**15.40**	—	**−13.75**	—	**23.98–31.21**
$A_a(0.9, 1.25, 1.5)$	15.40	—	−13.15	—	23.98–31.21
$A_p(0.9, 1.25, 1.5)$	15.40	—	−13.21	—	23.98–31.21

$r_M = 48.27\lambda$, $P = 5$ and $(\theta_0, \phi_0) = (90°, 0°)$.

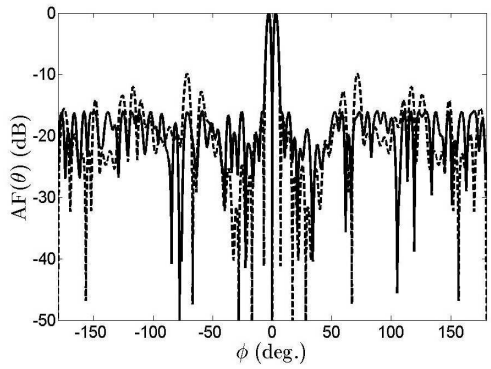

Figure 5. Difference pattern of dual-mode SCCAA's in the azimuth plane, $(\theta_0, \phi_0) = (90°, 0°)$, $M = 6$, $r_M = 48.27\lambda$, $P = 3$, solid curve (—): $A_g(0.9, 1.25, 1.5)$, dashed curve (− − −): $A_r(0.9, 1.25, 1.5)$.

1.5), achieves a better fitness of −56.57 dB while maintaining the same beamwidths, BW_s^a, BW_d^a and BW_s^e, of $A_r(0.9, 1.25, 1.5)$. As listed in Table 6, the GABCA achieves better fitness than the ABCA and the

PSO.

Next, consider $A_r(0.9,\ 1.25,\ 1.5)$ of $P = 5$ layers, with $(\theta_0, \phi_0) = (90°, 0°)$, $M = 6$, $r_M = 48.27\lambda$. The optimized arrays, $A_g(0.9,\ 1.25,\ 1.5)$, $A_a(0.9,\ 1.25,\ 1.5)$ and $A_p(0.9,\ 1.25,\ 1.5)$, are derived and summarized in Tables 5 and 7. Figs. 6 and 7 show the field patterns in the azimuth plane and the elevation plane of $A_r(0.9,\ 1.25,\ 1.5)$ and $A_g(0.9,\ 1.25,\ 1.5)$, respectively. The optimized array, $A_g(0.9,\ 1.25,\ 1.5)$, with the initial condition of $A_r(0.9,\ 1.25,\ 1.5)$, achieves a better fitness of -48.52 dB while maintaining the same beamwidths, BW_s^a, BW_d^a and

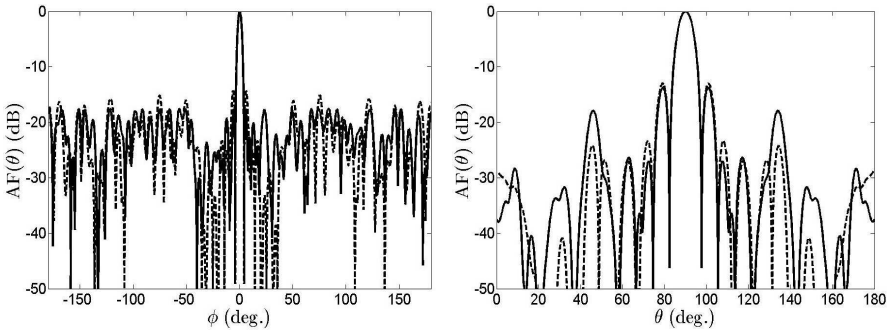

Figure 6. Sum pattern of dual-mode SCCAA's, (a) in the azimuth plane, (b) in the elevation plane, $(\theta_0, \phi_0) = (90°, 0°)$, $M = 6$, $r_M = 48.27\lambda$, $P = 5$, solid curve (—): $A_g(0.9,\ 1.25,\ 1.5)$, dashed curve $(- - -)$: $A_r(0.9,\ 1.25,\ 1.5)$.

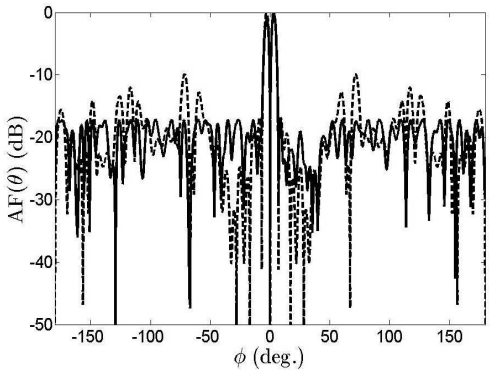

Figure 7. Difference pattern of dual-mode SCCAA's in the azimuth plane, $(\theta_0, \phi_0) = (90°, 0°)$, $M = 6$, $r_M = 48.27\lambda$, $P = 5$, solid curve (—): $A_g(0.9,\ 1.25,\ 1.5)$, dashed curve $(- - -)$: $A_r(0.9,\ 1.25,\ 1.5)$.

Table 6. Performance of GABCA, ABCA and PSO.

Algorithm	P_s^a (dB)	P_d^a (dB)	P_s^e (dB)	fitness (dB)	FI (times)
GABCA	−17.07	−15.09	−24.21	**−56.57**	392 000
ABCA	−14.35	−10.65	−17.13	−42.13	611 000
PSO	−15.85	−13.48	−19.51	−48.84	328 000

Parameters are the same as in Table 4.

Table 7. Performance of GABCA, ABCA and PSO.

Algorithm	P_s^a (dB)	P_d^a (dB)	P_s^e (dB)	fitness (dB)	FI (times)
GABCA	−17.57	−17.20	−13.75	**−48.52**	473 000
ABCA	−13.79	−10.67	−13.15	−37.61	12 000
PSO	−17.09	−14.64	−13.21	−44.94	523 000

Parameters are the same as in Table 5.

BW_s^e. As listed in Table 7, $A_g(0.9, 1.25, 1.5)$ has a better fitness than $A_a(0.9, 1.25, 1.5)$ and $A_p(0.9, 1.25, 1.5)$.

5. CONCLUSION

A stacked concentric circular antenna array (SCCAA) is proposed to provide dual-mode operation in the azimuth plane and narrower beamwidth in the elevation plane than CCAA's. A gbest-guided artificial bee colony algorithm (GABCA) is applied to optimize thinned SCCAA's in terms of reducing the side-lobe level while maintaining the beamwidth and the squint angle. The thinned SCCAA's have wider element spacings than regular SCCAA's, with the latter as the initial condition of optimization. The GABCA achieves better fitness than conventional ABCA and PSO in this task.

REFERENCES

1. Rudge, A. W., K. Milne, A. D. Olver, and P. Knight, *The Handbook of Antenna Design*, 2nd edition, 298–299, Inst. Engrg. Technol., 1983.
2. Panduro, M., A. L. Mendez, R. Dominguez, and G. Romero, "Design of non-uniform circular antenna arrays for side lobe reduction using the method of genetic algorithms," *Int. J. Electron. Commun.*, Vol. 60, 713–717, 2006.

3. Shihab, M., Y. Najjar, N. Dib, and M. Khodier, "Design of non-uniform circular antenna arrays using particle swarm optimization," *J. Elect. Eng.*, Vol. 59, No. 4, 216–220, 2008.
4. Panduro, M. A., C. A. Brizuela, L. I. Balderas, and D. A. Acosta, "A comparison of genetic algorithms, particle swarm optimization and the differential evolution method for the design of scannable circular antenna arrays," *Progress In Electromagnetics Research B*, Vol. 13, 171–186, 2009.
5. Roy, G. G., S. Das, P. Chakraborty, and P. N. Suganthan, "Design of non-uniform circular antenna arrays using a modified invasive weed optimization algorithm," *IEEE Trans. Antennas Propagat.*, Vol. 59, No. 1, 110–118, Jan. 2011.
6. Basu, B. and G. K. Mahanti, "Thinning of concentric two-ring circular array antenna using fire fly algorithm," *Scientia Iranica*, Vol. 19, No. 6, 1802–1809, Dec. 2012.
7. Yaacoub, E., M. Al-Husseini, A. Chehab, A. El Hajj, and K. Y. Kabalan, "Hybrid linear and circular antenna arrays," *Iran. J. Elec. Comput. Eng.*, Vol. 6, No. 1, 48–54, 2007.
8. Zhu, G. P. and S. Kwong, "Gbest-guided artificial bee colony algorithm for numerical function optimization," *Appl. Math. Comput.*, Vol. 217, No. 7, 3166–3173, Dec. 2010.
9. Basu, B. and G. K. Mahanti, "Fire fly and artificial bees colony algorithm for synthesis of scanned and broadside linear array antenna," *Progress In Electromagnetics Research B*, Vol. 32, 169–190, 2011.
10. Pan, Q.-K., L. Wang, K. Mao, J.-H. Zhao, and M. Zhang, "An effective artificial bee colony algorithm for a real-world hybrid flowshop problem in steelmaking process," *IEEE Trans. Autom. Sci. Eng.*, Vol. 10, No. 2, 307–322, Apr. 2013.
11. Robinson, J. and Y. Rahmat-Samii, "Particle swarm optimization in electromagnetics," *IEEE Trans. Antennas Propagat.*, Vol. 52, No. 2, 397–407, Feb. 2004.
12. Milligan, T. A., *Modern Antenna Design*, 2nd Edition, 196–202, Wiley-Interscience, 2005.
13. Mailloux, R. J., *Phased Array Antenna Handbook*, 2nd Edition, 132–133, Artech House, 2005.
14. Lo, Y. T. and S. W. Lee, *Antenna Handbook*, 13–29, van Nostrand Reinhold, 1988.
15. Balanis, C. A., *Antenna Theory*, 3rd edition, 50–52, John Wiley, 2005.